Indole Nucleophile Triggers Mechanistic Divergence in Ni-Photoredox N–Arylation

Kevin J. Liang,[#] Olivia R. Taylor,[#] Angie L. López, Russell J. Woo, and Ana Bahamonde*[a]

[a] K. J. Liang, O. R. Taylor,[#] A. L. López, R. J. Woo, and Dr. A. Bahamonde
Chemistry Department, University of California, Riverside
501 Big Springs Rd., Riverside, CA 92521 (USA)
E-mail: ana.bahamonde@ucr.edu

[#] Contributed equally to this manuscript

Supporting information for this article is given via a link at the end of the document

.

Abstract: This study presents a Ni-photoredox method for indole *N*-arylation, broadening the range of substrates to include indoles with unprotected C3-positions and base-sensitive groups. Through detailed mechanistic inquiries, a Ni(I/III) mechanism was uncovered, distinct from those commonly proposed for Ni-catalyzed amine, thiol, and alcohol arylation, as well as from the Ni(0/II/III) cycle identified for amide arylation under almost identical conditions. The key finding is the formation of a Ni(I) intermediate bearing the indole nucleophile as a ligand prior to oxidative addition, which is rare for Ni-photoredox carbon-heteroatom coupling and has a profound impact on the reaction kinetics and scope. The pre-coordination of indole renders a more electron-rich Ni(I) intermediate, which broadens the scope by enabling fast reactivity even with challenging electron-rich aryl bromide substrates. Thus, this work highlights the often-overlooked influence of X-type ligands on Ni oxidative addition rates and illustrates yet another mechanistic divergence in Ni-photoredox C–heteroatom couplings.

Introduction

Nickel-bipyridine photoredox catalysis has been established as a powerful strategy to afford a variety of C–heteroatom couplings at room temperature.[1] However, reports focused on mechanistic elucidation are scarce and complicated by the ease with which Ni can access many different oxidation states via electron transfers with the photocatalyst. Furthermore, the often-invoked odd-electron intermediates are difficult to isolate[2] and these systems present off-cycle Ni resting-states, which makes mechanistic investigations challenging.[3] In contrast, non-photochemically mediated Ni-heteroatom couplings have been extensively studied.[1e, 4] These systems employ stronger field ligands that allow for relatively stable on-cycle intermediates that can be isolated and detected by NMR or EPR analysis

Most Ni-photoredox reactions are proposed to proceed through the formation of a Ni(III) intermediate that undergoes fast C–heteroatom reductive elimination. When using highly nucleophilic substrates, such as amines, alcohols, and thiols, a Ni(I/III) mechanistic manifold has been shown to facilitate access to this Ni(III) intermediate (Figure 1a).[5] In this mechanism, all on-cycle intermediates are in low concentration and bimolecular Ni deactivation pathways compete with product formation. Alternatively, a Ni(0/II/III) mechanism was recently found by our group to predominate in amide arylation reactions (Figure 1b).[1e, 3, 6] While unclear at this stage, it was hypothesized that the lack of redox active base (shown to play a key role in the Ni(I/III) cycles),[3] together with the low nucleophilicity of amides, were responsible for the change in mechanism.[6e]

This paper describes the use of indoles as nitrogen nucleophiles. Given the similar pK_a values of amides and indoles,[7] we envisioned that our catalytic platform would be amenable for providing access to *N*-functionalized indole scaffolds via a similar Ni (0/II/III) pathway. Indeed, in this study, we demonstrate that indole *N*-arylation can be achieved under almost identical conditions to our previously reported amide arylation protocol. However, to our surprise, neither of the reported mechanisms depicted in Figure 1 are consistent with the experiments presented herein. Specifically, kinetic data supports the coordination of the indole to Ni(I) prior to oxidative addition. Thus, this study provides evidence for an additional pathway through which Ni-photoredox C–heteroatom coupling can occur.

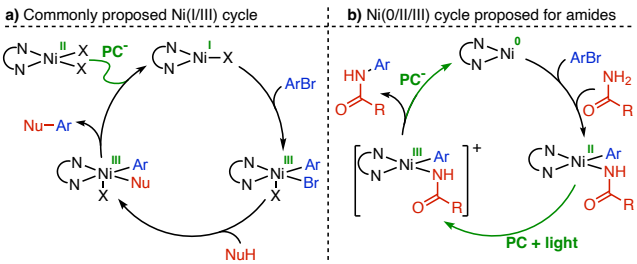

Figure 1. Catalytic cycles proposed for Ni-photoredox C-heteroatom reactions.

Beyond these mechanistic implications, this methodology provides an efficient means for decorating indoles, a central heterocyclic core in drug design.[8] In line with the recent report by the König and Paixão groups, which allows for the indole *N*-functionalization of tryptophan amino acids within a series of peptides,[9] high yields can be obtained for C3-substituted indoles. Notably, the methodology described in this paper also achieves

high yields and perfect selectivity when employing C3-unsubstituted indoles, which are known to readily undergo competing C3-funtionalization in the presence of electrophiles.[10] Furthermore, contrasting with other non-photoredox Ni-catalyzed couplings, high temperatures or strong *tert*-butoxide bases are not required, and thus base-sensitive groups like esters are tolerated.[4e-g]

Resultingly, we report both an attractive strategy to afford a large variety of indoles, and mechanistic investigations that showcases an unexpected mechanism. In doing so, this work provides clarity on the underlying causes that lead to mechanistic divergences for Ni-photoredox C–heteroatom couplings.

Results and Discussion

The reaction between 3-phenylindole and methyl 4-bromobenzoate was chosen as a model system to study indole *N*-arylation (Table 1, entry 1). To our delight, high product yields were quickly obtained with very minimal changes to the reaction conditions for our reported amide arylation protocol.[6d] Additionally, indole arylation was found to be much faster than amide arylation, with high yields obtained in as little as 3 hours, compared with the overnight reaction times required for amide arylation[6d] (entry 2). Such high reactivity prompted us to reduce the Ni loading, while still maintaining the 1:1.5 Ni to ligand ratio. The reactivity was found to be optimal at 5 mol% Ni, and interestingly both increasing and decreasing the Ni concentration from there led to decreased yields (entries 2-4). [3, 11] With the optimal conditions in hand, control experiments were performed to ensure that all the reaction components were required. No reactivity was observed in the absence of Ni, Ir photocatalyst (PC), or light (entries 5-7).

Table 1. Reaction optimization

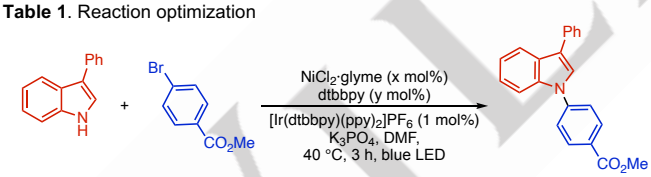

Entry	Ni loading	Ligand loading	Other variations	Yield[a]
1	10 mol%	15 mol%	24 h	79%
2	10 mol%	15 mol%	none	80%
3	5 mol%	7.5 mol%	none	91%
4	2.5 mol%	3.8 mol%	none	67%
5	-	-	none	n.d.
6	5 mol%	7.5 mol%	No Ir	n.d.
7	5 mol%	7.5 mol%	No light	n.d.

[a] Reaction conditions: $NiCl_2$·glyme (0.005-0.02 mmol), 4,4′-di-*tert*-butyl-2,2′-dipyridine (dtbbpy, 0.0075-0.03 mmol), $[Ir(dtbbpy)(ppy)_2]PF_6$ (0.002 mmol), K_3PO_4 (0.4 mmol), methyl 4-bromobenzoate (0.2 mmol), 3-phenylindole (0.3 mmol), and 1 mL of DMF, 40 °C, 3 h. All yields were determined by ^1H NMR analysis relative to 1,3,5-trimethoxybenzene as an internal standard.

Subsequently, indoles not bearing any C3-susbtitution were tested as substrates to assess the regioselectivity for *N*- vs. C3-arylation (Figure 2). Beginning with 1H-indole (**1a**), only one arylated indole product was detected in the crude reaction mixture. The isolated heterocyclic product was then analyzed by NMR and X-Ray crystallography to unambiguously confirm the formation of the *N*-arylated indole **3a**.[12] Furthermore, we were able to increase the scale to 2 mmol and still obtained an excellent 98% yield of **3a** after 48 hours.

Other 3-unsubstituted indoles were also tested and again showed exclusive selectivity for the formation of the *N*-functionalized indoles, with no C3 arylation products detected. Indoles bearing electron-donating and electron-withdrawing groups at C5 and C6 all generated the *N*-arylated products in moderated yields (**3b-3f**). Unsurprisingly, C3-substituted indoles were found to be excellent substrates for this reaction, rendering the arylated products in high yields (**3g-3h**). The results also show that protected amines and nitriles and base sensitive groups like esters, which are not tolerated in Ni-catalyzed thermal strategies,[4f, 4g] are tolerated.

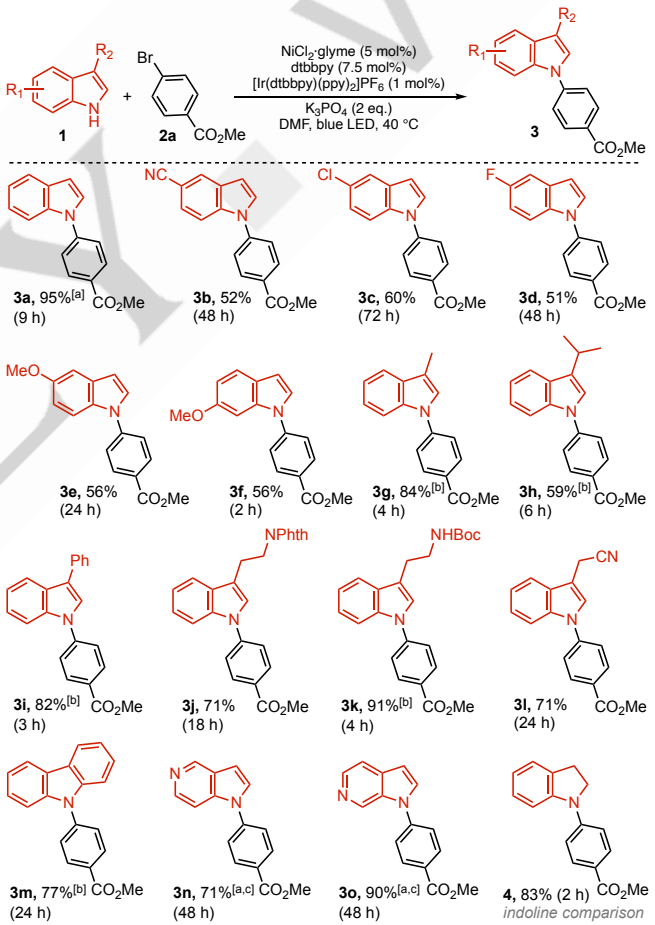

Figure 2. Scope of indole coupling partners in Ni-photoredox-catalyzed indole arylation. Reaction conditions: $NiCl_2$·glyme (0.01 mmol), 4,4′-di-*tert*-butyl-2,2′-dipyridine (dtbbpy, 0.015 mmol), $[Ir(dtbbpy)(ppy)_2]PF_6$ (0.002 mmol), K_3PO_4 (0.4 mmol), aryl bromide **2a** (0.2 mmol), indole **1** (0.3 mmol), and 1 mL of DMF, 40 °C. All reported values are yields of the isolated products. [a] Indole was used as limiting reagent: aryl bromide **2a** (0.4 mmol) and indole **1** (0.2 mmol). [b] $KHCO_3$ was used as base. [c] Ligand loading was reduced to 3.8 mol% (dtbbpy, 0.0075 mmol).

In contrast, highly nucleophilic groups like amines and alcohols are not tolerated, as they are also susceptible to arylation under these reaction conditions.[1b, 1c] Indoline was also tested as a comparison between the indole reactivity and that of a more nucleophilic amine with a similar steric profile. Faster reactivity was observed for indoline, presumably owing to its higher nucleophilicity, leading to 83% yield of **4** in 2 hours.

Other nitrogenated heterocycles related to indole were also arylated in high yields (**3m-3o**). Interestingly, when heterocycles bearing pyridine subunits were utilized, a lower ligand loading was found to be optimal (with reduced reactivity observed in the absence of added ligand). It is hypothesized that this is likely due to the propensity of these heterocycles to displace the bipyridine ligand used in these reactions. Lastly, sterically encumbered C2-substituted indoles were not tolerated under these reaction conditions.

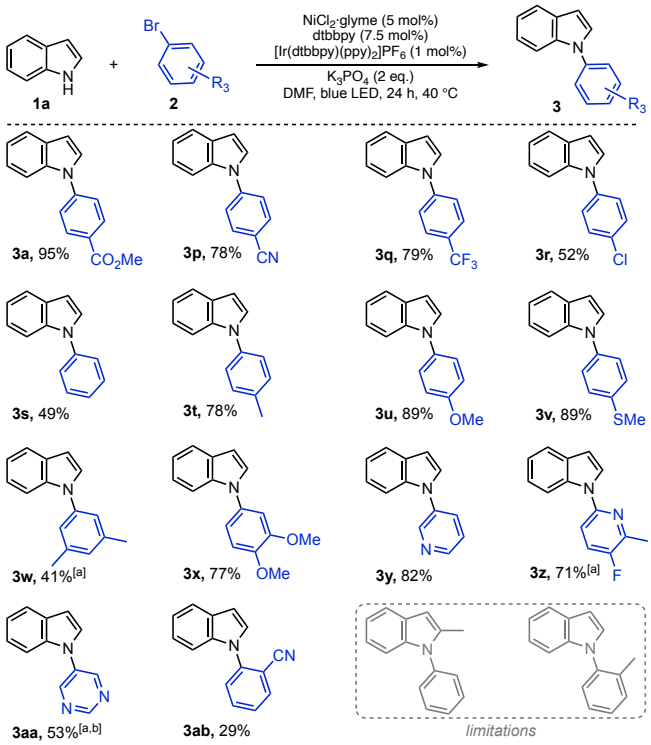

Figure 3. Scope of aryl bromide coupling partners in Ni-photoredox-catalyzed indole arylation. Reaction conditions: $NiCl_2$·glyme (0.01 mmol), 4,4′-di-*tert*-butyl-2,2′-dipyridine (dtbbpy, 0.015 mmol), $[Ir(dtbbpy)(ppy)_2]PF_6$ (0.002 mmol), K_3PO_4 (0.4 mmol), aryl bromide **2** (0.4 mmol), 1*H*-indole **1a** (0.2 mmol), and 1 mL of DMF, 40 °C, 24 h. All reported values are yields of the isolated products. [a] 48 h reaction time. [b] Aryl bromide **2** (0.6 mmol).

To better assess the generality of this reaction, unsubstituted 1H-indole (**1a**) was chosen as the substrate for investigating the aryl bromide scope (Figure 3). Once again, despite the presence of the unfunctionalized nucleophilic C3-position, perfect selectivity for the N-functionalization and high product yields were obtained. Substrates bearing ethers, thioethers, esters, and nitriles were tolerated (**3u**, **3v**, **3a**, and **3p**, respectively). Additionally, no reactivity was observed when aryl chlorides were used. This allowed us to use aryl bromides bearing chlorine atoms with no chloride loss detected (**3r**). Lastly, pyridine and pyrimidine heterocycles, which are often found in commercial drugs,[8b] were also suitable coupling partners (**3y-3aa**).

To our surprise, and in contrast to most Ni-catalyzed arylation reactions,[1e] the electronics of the aryl halide had very little effect on the reaction yield, with high yields achieved for both electron-rich and electron-poor substrates after 24 hours of reaction time (**3a, 3p-3v**).[13] This is in stark contrast to the 7 days of reaction time required for the arylation of amides with electron-rich aryl bromides like 1-bromo-4-methoxybenzene.[6d] Intrigued by this unusual, yet desirable behavior, an in-depth study of the oxidative addition step was conducted and will be described later in the manuscript.

In contrast to the limited effect of aryl electronics on the reaction yield, sterically hindered aryl bromides (**3ab**) were found to have a substantial influence on reactivity. These substrates displayed low conversions and yields, and, unlike for our prior work with amide arylation,[6d] longer reaction times did not lead to higher yields.

At the outset of our investigation, it was expected that analogous reactivity to the Ni-photoredox amide arylation recently reported by our lab would be observed. However, during our scope and optimization studies, several surprising differences were observed relative to our prior amide arylation chemistry.[6d, 6e] These different reactivity patterns suggested to us that, despite the similar reaction conditions and substrate pK_a values,[7] a different mechanism may be operative in each system. Specifically, during the indole arylation optimization the Ni loading exhibited an activity “sweet spot” at 5 mol%, with higher and lower loadings leading to reduced yields. In contrast, for amide arylation both 10 and 20 mol% of Ni gave similar product yields and outperformed reactions carried out with 5 mol% Ni or lower. Additionally, aryl bromide electronics had little effect on indole arylation, and substantial inhibition of reactivity was seen for sterically hindered substrates (Figure 3). These observations again differ from the reactivity displayed by amides, where long reaction times (up to 7 days) were required for electron-rich and sterically hindered aryl bromides, but high yields were attainable after these prolonged reactions.[6d]

These intriguing observations prompted us to pursue mechanistic studies. To avoid possible side reactions which can be facilitated by the reactivity of soluble organic bases,[3] the optimized reaction conditions were not modified for the mechanistic studies. The heterogeneity of the system thus impeded the calculation of accurate quantum yields. Despite this complexity, we hypothesized that we could leverage our experience in kinetic measurements of photochemical systems to interrogate the reaction mechanism.[6e] To ensure that different kinetic runs can be reliably compared to each other, all kinetic runs were performed by carrying out two side-by-side reactions. One reaction was kept constant with the optimized conditions, while the other contained the variations in the reaction conditions that were being studied. Additionally, every measurement on every plot was performed the same day and using the same stock solutions. This way, every set of reactions can be compared, and

the system reproducibility is tested every run against the model reaction kinetics. Finally, all the measurements were repeated on a different day with fresh stock solutions.

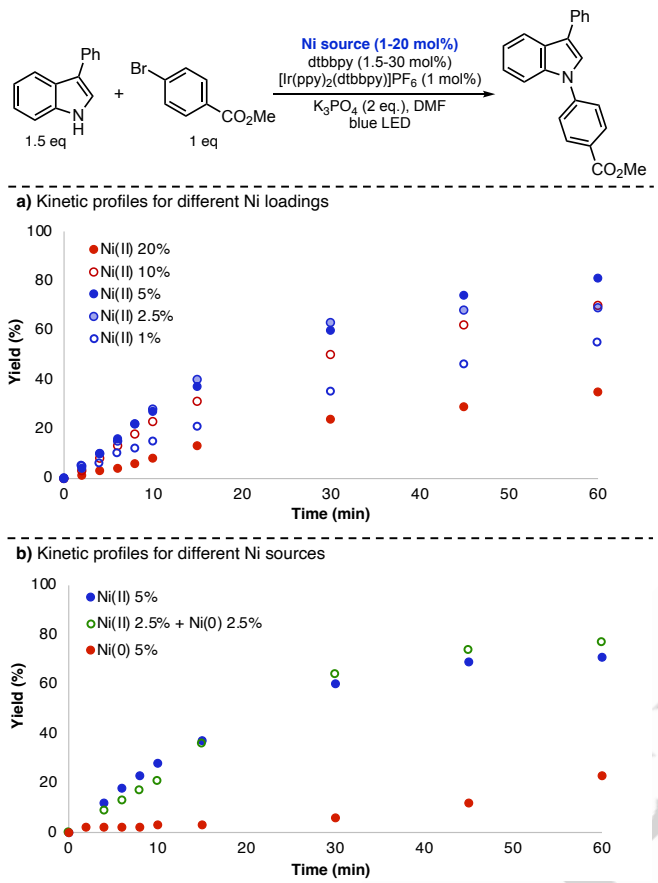

Figure 4. (a) Effect of Ni concentration on reaction rate. (b) Effect of different Ni pre-catalysts on reaction rate. Reaction conditions: $NiCl_2$·glyme (0.002 to 0.04 mmol) or $Ni(COD)_2$ (0.005 to 0.01 mmol), 4,4′-di-*tert*-butyl-2,2′-dipyridine (dtbbpy, 0.003 to 0.06 mmol), $[Ir(dtbbpy)(ppy)_2]PF_6$ (0.002 mmol), K_3PO_4 (0.4 mmol), methyl 4-bromobenzoate (0.2 mmol), 3-phenylindole (0.3 mmol), and 1 mL of DMF. All yields were determined in duplicate by ^1H NMR analysis.

We began by investigating the effect of the Ni pre-catalyst and loading on the reaction rate. Mirroring the behavior observed for the final reaction yield, the reaction rate increased as $NiCl_2$·glyme loading was increased from 1 mol% to 5 mol% (blue points, Figure 4a), but higher loadings led to slower rates (red points, Figure 4a). This behavior contrasted with the kinetic profiles measured for our amide arylation system, where zero order dependence on Ni and an extended induction period were observed.[6e] To better understand the differences between this reaction mechanism and the amide arylation, which we had expected to have identical mechanisms, we then decided to compare the reactivity of different pre-catalysts. We were especially intrigued about the kinetics for a Ni(0) pre-catalyst, which was optimal for the amide arylation protocol, providing fast kinetics with no induction period.

We first tested if (dtbbpy)Ni(COD) was a suitable pre-catalyst for indole arylation and observed a 29% yield of the arylated indole after 24 h. Under these conditions, the reaction kinetics showed a marked induction period (Figure 4b, red points). It should be noted that the procedure used here was identical to that used when studying the amide arylation system. This suggests that displacement of the COD ligand is not likely to be responsible for the sluggish kinetics observed for indole arylation.

Finally, a mix of these Ni(II) and Ni(0) complexes was tested as the pre-catalyst. This mixture has been shown to quickly generate Ni(I) in situ,[6e] and displayed an induction period and slow kinetics when used in the amide arylation chemistry. As shown by the green circles (Figure 4b), a different behavior from that measured for the amide chemistry was once again observed. In this case, an overlap between the Ni(II) and the Ni(II) + Ni(0) mixture was observed.

Taken together, these experiments indicate that a Ni(0/II/III) cycle is not prevalent for this system and suggest that a Ni(I/III) cycle is predominant for this chemistry. Specifically, a Ni(0/II/III) cycle, as identified for amide arylation,[6e] would present faster kinetics when Ni(0) is used as the pre-catalyst, and the Ni(II) + Ni(0) mixture would be expected to render slower kinetics than the reactions carried out with Ni(0) alone. Finally, the “sweet spot” behavior measured for different Ni loadings has been also observed in other photoredox Ni(I)-catalyzed reactions where higher quantum yields were observed at lower Ni loadings.[3, 11, 14] The lower reactivity at high Ni loadings has been attributed to faster formation of off-cycle Ni(II) and Ni(0) species via comproportionation and disproportionation events between Ni(I) and Ni(III) intermediates. As a result, these side reactions have a quadratic dependence on Ni concentration.

Finally, the reaction rate was found to have no dependence on the photocatalyst and indole concentrations (see SI, Figures S6 and S7). Other than Ni loading, only the aryl bromide concentration had an effect on the reaction rate, displaying saturation kinetics (see SI, Figures S8 to S9), which suggests a turnover-limiting oxidative addition step.

To further probe the possibility of a Ni(I/III) cycle, we tested if the indole could play a dual role as a coupling partner and as the terminal reductant for the Ir photocatalyst.[9] Stern-Volmer quenching experiments demonstrated that indoles are indeed able to participate in both cycles and serve as the reductant for the photocatalyst (see SI for details). Other pathways for accessing Ni(I) though photolysis of Ni(II) intermediates have been demonstrated via stoichiometric studies of related systems.[2b, 15] It is hypothesized that these are likely to also be operative, such that multiple mechanisms for the generation of Ni(I) are concurrent under our reaction conditions. This study has not focused on better understanding the specific nature of this initiation step given the extensive literature on this subject, along with the fact that photocatalyst concentration was found not to influence the reaction rate. Although the heterogeneity of the system precluded us from performing quantum yield measurements, kinetic studies revealed a small but positive effect of the light intensity that is consistent with a radical chain reaction.

With this information in hand, and based on previous studies for other C–heteroatom Ni-photoredox reactions,[1e, 3, 14, 15b] the preliminary mechanism depicted in Figure 5 became our working hypothesis to further study the system. The formation of the key

Ni(III) intermediate **B**, thought to be responsible for the C–N bond formation, is proposed to be accessed from Ni(I) intermediate **A**. Under our reaction conditions, X would be a chloride in the first turnover and a bromide thereafter. At this stage, two different pathways from **A** to **C** can be proposed: Pathway A, where oxidative addition precedes ligand exchange and intermediate **B** is formed, and Pathway B, where first the indole coordinates to the Ni(I) complex and intermediate **D** undergoes oxidative addition.

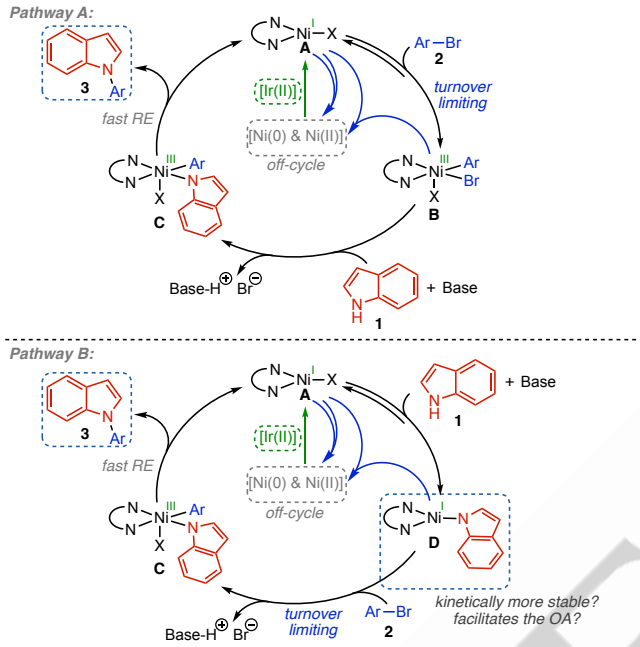

Figure 5. General schemes for the proposed Ni(I/III) mechanisms and possible order of oxidative addition (OA) and ligand exchange.

The kinetic data presented up to this point is consistent with both pathways, where either the oxidative addition **A** → **B** or **D** → **C** would be the turnover-limiting step of the reaction. While differentiating between these two options has not been thoroughly studied within the realm of Ni-photoredox catalysis, Pathway A has been proposed for most C–heteroatom couplings.[3, 6b, 9, 14, 16] However, it was unclear to us why indoles would preferentially react via a Ni(I/III) cycle and amides would not, since product formation results in the common intermediate **A** in both cases, which would undergo rate-limiting oxidative addition analogously. On the other hand, the generation of intermediates which bear the nucleophile prior to oxidative addition, analogous to **D**, are rarely invoked. Intermediates analogous to **D** have only been proposed in the arylation of amines and thiols with aryl iodides.[17] It should be noted that these reactions are proposed to undergo a different mechanism, where a heteroatom-centered radical is trapped by a Ni(I)complex and intermediate **D** is access though reduction of a Ni(II) complex. Given the high instability of the indole radical, if this previously proposed mechanism were operative under our reaction conditions, it would require a high concentration of the Ni(I) complex to enable the trapping. This is inconsistent with our in-situ EPR studies, which show no Ni(I) signal.

Although Pathway B is, to our knowledge, unprecedented for Ni-photoredox C–heteroatom couplings, the coordination of the indole prior to oxidative addition has been observed in other Cu-catalyzed C–N couplings.[18] Thus we wondered if the formation of intermediate **D** was the key step that triggers the switch in mechanism for indoles. It would be expected that the more electron-rich complex **D** would undergo faster oxidative addition into the aryl bromide compared to complex **A**.[13] Additionally, the steric environment around the Ni center in **D** may slow down undesired comproportionation pathways and can explain the diminished reactivity observed with sterically encumbered substrates. It should be noted that the coordination of nitrogenated substrates to Ni(I) complexes prior to oxidative addition has been reported by Matsubara using NHC ligands.[4c] Intriguingly, the synthesis of a NHC Ni(I) complex bearing an indole ligand was described, but when using this different ligand system reactivity was only observed under stoichiometric conditions and no product formation was detected under the optimized catalytic conditions.[4c] This highlights the different reactivities that are observed for Ni depending on the ancillary ligand.

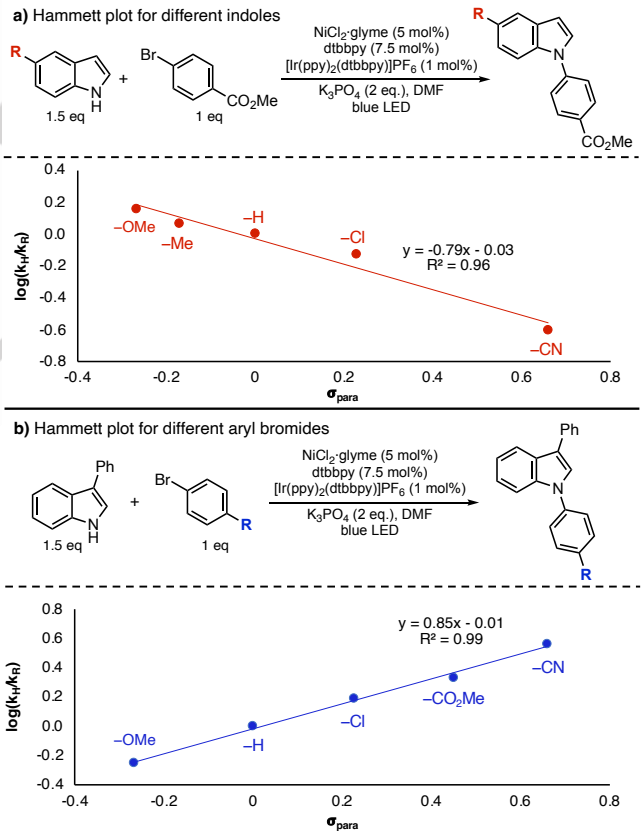

Figure 6. (a) Effect of indole electronics on the reaction rate. (b) Effect of aryl bromide electronics on reaction rate. Reaction conditions: $NiCl_2$·glyme (0.01 mmol), 4,4′-di-*tert*-butyl-2,2′-dipyridine (dtbbpy, 0.015 mmol), Ir[(dtbbpy)(ppy)$_2$]PF_6 (0.002 mmol), K_3PO_4 (0.4 mmol), aryl bromide (0.2 mmol), indole (0.3 mmol), and 1 mL of DMF. All yields were determined by ^{1}H NMR analysis.

To differentiate between Pathways A and B, we studied the effect of the indole electronics on the reaction rate. If Pathway B is

operative, the absence of the indole concentration from the rate law would be due to saturation kinetics and faster rates would be expected when more electron-rich indoles are used due to the faster rate of oxidative addition (**D** → **C**). Alternatively, if Pathway A is operative, varying the indole electronics would not be expected to impact the reaction rate, as indole enters the cycle after the turnover-limiting step. It should be noted that, although the indole is involved in two different steps, it would not be expected that changes in the indole electronic properties would influence the overall rate by changing the photocatalyst quenching rate. This is because the order in photocatalyst is zero, and the indole is used in a large excess with respect to the photocatalyst.

The reaction rates of a series of indoles bearing different substituents in the C5-position were measured. As shown in Figure 6a, a clear correlation between the indole electronics and the reaction rate was observed, supporting the involvement of the indole at or before the turnover-limiting step. Additionally, the effect of the aryl bromide electronics on the reaction rate was also measured, and a positive slope was observed (Figure 6b). This is in line with previous Ni-catalyzed oxidative addition Hammett studies.[13]

Figure 5 summarizes the findings of our mechanistic studies, where the Ni(I/III) cycle in Pathway B is proposed for generating the arylated indole products. Indole coordination prior to oxidative addition is supported by the Hammett studies depicted in Figure 6a and provides a rationale as to why the reaction scope tolerates a range of electronic profiles in the aryl bromide partner but is very sensitive to steric bulk. Upon the formation of **D**, a turnover-limiting oxidative addition is proposed to render Ni(III) intermediate **C**. A fast reductive elimination (RE) from this highly reactive intermediate yields the product and regenerates Ni(I) intermediate **A**.[5] At this stage, a competing direct oxidative addition from **A** to enable product formation via Pathway A (Figure 5) cannot be definitively discarded. However, the distinct effect of the indole electronics on the reaction rate suggests that formation of **D** prior to oxidative addition is the dominant pathway.

Finally, the slower kinetics observed for Ni loadings higher than 5 mol% are consistent with competing side reactions that have second order dependence on Ni and yield off-cycle Ni complexes (blue arrows, Figure 5). This behavior has also been observed in other Ni(I/III) catalytic cycles and is attributed to comproportionation and disproportionation events between the Ni(I) and Ni(III) intermediates. Indeed, when aliquots of the reaction were analyzed by EPR spectroscopy, no signal was detected, suggesting that a large portion of Ni is sequestered off-cycle. Lastly, as shown in previous studies[3, 6b, 9, 14, 16] and in line with our Stern-Volmer quenching experiments, the necessity for constant light irradiation (SI S13 and S5, respectively) is attributed to the photochemically mediated reduction of Ni(II) off-cycle species back into the catalytic cycle.

Conclusion

In summary, the development of a Ni-photoredox protocol for indole *N*-arylation is described. The substrate scope includes a large variety of examples where the potentially reactive indole C3-position is unprotected and base-sensitive substrates are used. Additionally, mechanistic studies revealed a Ni(I/III) mechanism, where a Ni(I) intermediate bearing the indole nucleophile as a ligand is formed prior to oxidative addition. This mechanistic manifold contrasts with both the Ni(I/III) mechanism proposed for Ni-catalyzed amine, thiol, and alcohol arylation, where Ni(I) halide (**A**) is proposed to directly undergo oxidative addition,[3, 6b, 9, 14, 16] and the Ni(0/II/III) cycle identified under analogous conditions for amide arylation reactions.[6d, 6e]

It is hypothesized that the rate of ligand exchange to form intermediate **D**, together with its ability to facilitate oxidative addition, are key factors for favoring the mechanism depicted in Pathway B (Figure 5). At this stage, the generality of this mechanism is unclear, as are the specific features of the nitrogen coupling partner that favor it. However, we believe that this manifold may not be restricted to only indole nucleophiles, and further studies to discern the underlying features of the heteroatom coupling partner that govern these mechanistic divergences are currently ongoing in our laboratory. We anticipate that the findings of this paper will help inform future catalyst development for carbon–heteroatom bond formation by highlighting the potential influence of X-type donors on the Ni(I) oxidative addition rate.

Experimental Section

General procedure for indole N-arylation: An oven-dried 10 mL Schlenk tube was charged with a magnetic stir bar and capped with a ground glass stopper. The reaction vessel was evacuated and refilled with nitrogen gas. Solid reagents were added to the Schlenk tube via paper cone under a constant flow of nitrogen gas. The vessel was charged with [Ir(dtbbpy)(ppy)2]PF6 (1.8 mg, 0.002 mmol), NiCl2·glyme (2.2 mg, 0.01 mmol), 4,4'-di-tert-butyl-2,2'-dipyridyl (4.0 mg, 0.015 mmol), indole 1 (0.2 mmol), aryl bromide 2 (0.2 mmol), and K3PO4 (84.9 mg, 0.4 mmol). After addition of the solids, the reaction vessel was evacuated and refilled with nitrogen gas three times. 1.0 mL of dimethylformamide, obtained from an SPS solvent system, was added to the reaction vessel under constant efflux of nitrogen gas. For liquid substrates, the liquid was added to the reaction flask after the addition of the solvent, still under constant nitrogen flow. The ground glass stopper was coated in vacuum grease before sealing the reaction vessel, and the stopper was subsequently wrapped in parafilm. The reaction vessel was placed 1 inch in front of a 427 nm Kessil LED lamp while being submerged in a temperature-controlled water bath in a crystallizing dish held at a constant 40 °C. After 3 hours, a second equivalent of aryl bromide 2 (0.2 mmol) was added to the reaction vessel. The Schlenk flask was subsequently resealed and then placed back in front of the lamp for the remaining reaction time.

Upon completion, the reaction mixture was filtered through a pad of celite using dichloromethane or ethyl acetate. The crude filtrate was concentrated in vacuo and adsorbed onto a small amount of silica. This material was loaded dry onto a chromatography column and the arylated indole product was isolated.

Supporting Information

The authors have cited additional references within the Supporting Information.[19], [20], [21], [22], [23], [24], [25], [26]

Acknowledgements

The authors thank Lingchao Zhu for his assistance with the EPR measurements and Veronica Carta for her assistance with the X-Ray measurements. This work was supported by the NSF (CHE-2235778) and the University of California, Riverside.

Keywords: indole functionalization • Ni-photoredox • mechanistic study

[1] a) C. Zhu, H. Yue, J. Jia, M. Rueping, *Angew. Chem. Int. Ed.* **2020**, *133*, 17954-17975; b) J. A. Terrett, J. D. Cuthbertson, V. W. Shurtleff, D. W. MacMillan, *Nature* **2015**, *524*, 330-334; c) E. B. Corcoran, M. T. Pirnot, S. Lin, S. D. Dreher, D. A. DiRocco, I. W. Davies, S. L. Buchwald, D. W. MacMillan, *Science* **2016**, *353*, 279-283; d) E. R. Welin, C. Le, D. M. Arias-Rotondo, J. K. McCusker, D. W. MacMillan, *Science* **2017**, *355*, 380-385; e) O. R. Taylor, P. J. Saucedo, A. Bahamonde, *J. Org. Chem.* **2024**.

[2] a) S. I. Ting, W. L. Williams, A. G. Doyle, *J. Am. Chem. Soc.* **2022**, *144*, 5575-5582; b) E. Sutcliffe, D. A. Cagan, R. G. Hadt, *J. Am. Chem. Soc.* **2024**, *146*, 15506-15514; c) E. L. Johnson Humphrey, A. R. Kennedy, S. Sproules, D. J. Nelson, *European Journal of Inorganic Chemistry* **2022**, *2022*, e202101006; d) Q. Lin, T. Diao, *J. Am. Chem. Soc.* **2019**, *141*, 17937-17948; e) R. J. Somerville, C. Odena, M. F. Obst, N. Hazari, K. H. Hopmann, R. Martin, *J. Am. Chem. Soc.* **2020**, *142*, 10936-10941; f) M. Mohadjer Beromi, G. W. Brudvig, N. Hazari, H. M. Lant, B. Q. Mercado, *Angew. Chem. Int. Ed.* **2019**, *58*, 6094-6098; g) D. C. Powers, B. L. Anderson, D. G. Nocera, *J. Am. Chem. Soc.* **2013**, *135*, 18876-18883.

[3] a) N. A. Till, L. Tian, Z. Dong, G. D. Scholes, D. W. MacMillan, *J. Am. Chem. Soc.* **2020**, *142*, 15830-15841; b) R. Sun, Y. Qin, S. Ruccolo, C. Schnedermann, C. Costentin, D. G. Nocera, *J. Am. Chem. Soc.* **2019**, *141*, 89-93.

[4] a) J. B. Diccianni, T. Diao, *Trends Chem.* **2019**, *1*, 830-844; b) M. Marin, R. J. Rama, M. C. Nicasio, *The Chemical Record* **2016**, *16*, 1819-1832; c) T. Inatomi, Y. Fukahori, Y. Yamada, R. Ishikawa, S. Kanegawa, Y. Koga, K. Matsubara, *Catalysis Science & Technology* **2019**, *9*, 1784-1793; d) M. I. Lipschutz, X. Yang, R. Chatterjee, T. D. Tilley, *J. Am. Chem. Soc.* **2013**, *135*, 15298-15301; e) N. H. Park, G. Teverovskiy, S. L. Buchwald, *Org. Lett.* **2014**, *16*, 220-223; f) S. G. Rull, J. F. Blandez, M. R. Fructos, T. R. Belderrain, M. C. Nicasio, *Adv. Synth. Catal.* **2015**, *357*, 846-846; g) R. T. McGuire, J. F. J. Paffile, Y. Zhou, M. Stradiotto, *ACS Catal.* **2019**, *9*, 9292-9297.

[5] a) K. Koo, G. L. Hillhouse, *Organometallics* **1995**, *14*, 4421-4423; b) K. Koo, G. L. Hillhouse, *Organometallics* **1996**, *15*, 2669-2671; c) R. Han, G. L. Hillhouse, *J. Am. Chem. Soc.* **1997**, *119*, 8135-8136; d) B. L. Lin, C. R. Clough, G. L. Hillhouse, *J. Am. Chem. Soc.* **2002**, *124*, 2890-2891; e) F. Le Vaillant, E. J. Reijerse, M. Leutzsch, J. Cornella, *J. Am. Chem. Soc.* **2020**, *142*, 19540-19550.

[6] a) Y. Ben-Tal, G. C. Lloyd-Jones, *J. Am. Chem. Soc.* **2022**, *144*, 15372-15382; b) C. H. Chrisman, M. Kudisch, K. O. Puffer, T. K. Stewart, Y. M. L. Lamb, C.-H. Lim, R. Escobar, P. Thordarson, J. W. Johannes, G. M. Miyake, *J. Am. Chem. Soc.* **2023**, *145*, 12293–12304; c) C. Zhu, H. Yue, P. Nikolaienko, M. Rueping, *CCS Chemistry* **2020**, *2*, 179-190; d) R. D. Bradley, A. Bahamonde, *Org. Lett.* **2022**, *24*, 7134-7139; e) R. D. Bradley, B. D. McManus, J. G. Yam, V. Carta, A. Bahamonde, *Angew. Chem. Int. Ed.* **2023**, *62*, e202310753.

[7] F. G. Bordwell, *Acc. Chem. Res.* **1988**, *21*, 456-463.

[8] a) M.-Z. Zhang, Q. Chen, G.-F. Yang, *European journal of medicinal chemistry* **2015**, *89*, 421-441; b) R. D. Taylor, M. MacCoss, A. D. Lawson, *J. Med. Chem.* **2014**, *57*, 5845-5859; c) A. Majumder, R. Gupta, M. Mandal, M. Babu, D. Chakraborty, *J. Organomet. Chem.* **2015**, *781*, 23-34; d) G. Sarkar, N. Bandopadhyay, K. Paramanik, S. Saha, S. J. Panda, C. S. Purohit, B. Biswas, H. S. Das, *Molecular Catalysis* **2023**, *545*, 113212; e) D.-X. Bai, R. S.-E. Lim, H.-F. Ng, Y.-C. Teo, *Synthetic Communications* **2021**, *51*, 1398-1405; f) S. Sil, A. Santha Bhaskaran, S. Chakraborty, B. Singh, R. Kuniyil, S. K. Mandal, *J. Am. Chem. Soc.* **2022**, *144*, 22611-22621; g) G. N. Vaidya, A. Khan, H. Verma, S. Kumar, D. Kumar, *J. Org. Chem.* **2019**, *84*, 3004-3010; h) A. R. Hajipour, F. Dordahan, F. Rafiee, *Applied Organometallic Chemistry* **2013**, *27*, 704-706.

[9] J. A. C. Delgado, Y.-M. Tian, M. Marcon, B. König, M. W. Paixão, *J. Am. Chem. Soc.* **2023**, *145*, 26452-26462.

[10] a) R. Van Order, H. Lindwall, *Chem. Rev.* **1942**, *30*, 69-96; b) N. A. Shafakat Ali, B. Ahmad Dar, V. Pradhan, M. Farooqui, *Mini reviews in medicinal chemistry* **2013**, *13*, 1792-1800; c) P. Bhattacharjee, U. Bora, *Organic Chemistry Frontiers* **2021**, *8*, 2343-2365; d) M. Bandini, *Org. Biomol. Chem.* **2013**, *11*, 5206-5212.

[11] L. Griego, J. B. Chae, L. M. Mirica, *Chem* **2024**.

[12] Deposition number 2345342 (for 3a) contain the supplementary crystallographic data for this paper. These data are provided free of charge by the joint Cambridge Crystallographic Data Centre and Fachinformationszentrum Karlsruhe Access Structures service.

[13] a) C. N. Pierson, J. F. Hartwig, *Nat. Chem.* **2024**, 1-8; b) S. I. Ting, W. L. Williams, A. G. Doyle, *J. Am. Chem. Soc.* **2022**, *144*, 5575-5582.

[14] Y. Qin, R. Sun, N. P. Gianoulis, D. G. Nocera, *J. Am. Chem. Soc.* **2021**, *143*, 2005-2015.

[15] a) D. A. Cagan, D. Bím, B. Silva, N. P. Kazmierczak, B. J. McNicholas, R. G. Hadt, *J. Am. Chem. Soc.* **2022**, *144*, 6516-6531; b) D. A. Cagan, D. Bím, N. P. Kazmierczak, R. G. Hadt, *ACS Catal.* **2024**, *14*, 9055-9076.

[16] Y. Kawamata, J. C. Vantourout, D. P. Hickey, P. Bai, L. Chen, Q. Hou, W. Qiao, K. Barman, M. A. Edwards, A. F. Garrido-Castro, *J. Am. Chem. Soc.* **2019**, *141*, 6392-6402.

[17] a) J. Santandrea, C. Minozzi, C. Cruché, S. K. Collins, *Angew. Chem. Int. Ed.* **2017**, *56*, 12255-12259; b) M. S. Oderinde, M. Frenette, D. W. Robbins, B. Aquila, J. W. Johannes, *J. Am. Chem. Soc.* **2016**, *138*, 1760-1763; c) C. Zhu, H. Yue, J. Jia, M. Rueping, *Angew. Chem. Int. Ed.* **2021**, *133*, 17954-17975; d) M. S. Oderinde, N. H. Jones, A. Juneau, M. Frenette, B. Aquila, S. Tentarelli, D. W. Robbins, J. W. Johannes, *Angew. Chem. Int. Ed.* **2016**, *128*, 13413-13417.

[18] D. T. Ziegler, J. Choi, J. M. Muñoz-Molina, A. C. Bissember, J. C. Peters, G. C. Fu, *J. Am. Chem. Soc.* **2013**, *135*, 13107-13112.

[19] C. J. O'Brien, D. G. Droege, A. Y. Jiu, S. S. Gandhi, N. A. Paras, S. H. Olson, J. Conrad, *J. Org. Chem.* **2018**, *83*, 8926-8935.

[20] J. R. Rizzo, C. A. Alt, T. Y. Zhang, *Tetrahedron Lett.* **2008**, *49*, 6749-6751.

[21] M. Bhuyan, B. Koenig, *Chem. Comm.* **2012**, *48*, 7489-7491.

[22] P. Caramenti, R. K. Nandi, J. Waser, *Chem. Eur. J.* **2018**, *24*, 10049-10053.

[23] SAINT, V8.30A, Bruker Analytical X-Ray Systems, Madison, WI, 2012.

[24] SADABS, 2.03, Bruker Analytical X-Ray Systems, Madison, WI, 2016.

[25] a) Sheldrick, G. M. Acta Cryst 2008, A64, 112. b) Sheldrick, G. M. Acta Cryst 2015, A71, 3.

[26] O. V. Dolomanov, L. J. Bourhis, R. J. Gildea, J. A. Howard, H. Puschmann, *J. Appl. Crystallogr.* **2009**, *42*, 339-341.

Entry for the Table of Contents